10-15-1993

Orientational Phases for M_3C_{60}

Taner Yildirim
University of Pennsylvania, taner@seas.upenn.edu

Suklyun Hong
University of Pennsylvania

A. Brooks Harris
University of Pennsylvania, harris@sas.upenn.edu

Eugene J. Mele
University of Pennsylvania, mele@physics.upenn.edu

Recommended Citation

Yildirim, T., Hong, S., Harris, A., & Mele, E. J. (1993). Orientational Phases for M_3C_{60}. *Physical Review B, 48* (16), 12262-12277. http://dx.doi.org/10.1103/PhysRevB.48.12262

Orientational Phases for M_3C_{60}

Abstract

The mechanism of the orientational ordering of C_{60} in alkali-metal-doped fullerenes M_3C_{60} is studied. Since the *M*-C_{60} (*M*=K,Rb) interactions cause the C_{60} molecules to assume one of two standard orientations, this model is equivalent to a generalized Ising model on a fcc lattice. The Ising interactions depend on two type of energies: (1) the direct interaction, i.e., the orientationally dependent part of interactions between nearest-neighboring C_{60} molecules (each carrying charge -3*e*), and (2) the band energy of the electrons transferred from M^+ ions to the C_{60}^{3-} ions. It is shown that the contribution to the pairwise interaction from the direct orientational interaction is ferromagnetic and dominantly nearest neighbor. However, contributions from the band (kinetic) energy of the conduction electrons are found to be antiferromagnetic for first- and third-nearest neighbors, ferromagnetic for second- and fourth-nearest neighbors, and negligible for further neighbors. The total first-neighbor interaction is probably antiferromagnetic. a non-negligible four-spin interaction is also obtained. The implication of these results for the orientational structure is discussed.

Disciplines

Physics

Orientational phases for M_3C_{60}

T. Yildirim, S. Hong, A. B. Harris, and E. J. Mele
Department of Physics, University of Pennsylvania, Philadelphia, Pennsylvania 19104-6396
(Received 4 February 1993; revised manuscript received 10 June 1993)

The mechanism of the orientational ordering of C_{60} in alkali-metal-doped fullerenes M_3C_{60} is studied. Since the M-C_{60} (M = K, Rb) interactions cause the C_{60} molecules to assume one of two standard orientations, this model is equivalent to a generalized Ising model on a fcc lattice. The Ising interactions depend on two type of energies: (1) the direct interaction, i.e., the orientationally dependent part of interactions between nearest-neighboring C_{60} molecules (each carrying charge $-3e$), and (2) the band energy of the electrons transferred from M^+ ions to the $C_{60}{}^{3-}$ ions. It is shown that the contribution to the pairwise interaction from the direct orientational interaction is ferromagnetic and dominantly nearest neighbor. However, contributions from the band (kinetic) energy of the conduction electrons are found to be antiferromagnetic for first- and third-nearest neighbors, ferromagnetic for second- and fourth-nearest neighbors, and negligible for further neighbors. The total first-neighbor interaction is probably antiferromagnetic. A non-negligible four-spin interaction is also obtained. The implication of these results for the orientational structure is discussed.

I. INTRODUCTION

The fullerenes represent interesting systems from both fundamental and applied points of view. In undoped C_{60} the cooperative ordering of the molecular orientations, which takes place at a temperature of about 250 K,[1] represents an interesting statistical mechanical system. In this system the orientational order parameter has unusually high symmetry: it transforms like a sixth-order spherical harmonic.[2] At much lower temperatures, the orientational dynamics undergoes freezing possibly via a phase transition at about 90 K.[3] Other fullerenes also show intriguing orientational behavior. In pure C_{70},[4] for instance, the orientational ordering develops in stages via two phase transitions. In the doped systems, there is less evidence of thermodynamic phase transitions involving orientational ordering. As we will discuss below, the orientational potential acting on the C_{60} molecules has a larger angular dependence, thus creating barriers that inhibit the existence of an equilibrium phase transition associated with molecular orientations. In extreme cases, i.e., for low doping of Na, the Na-C_{60} interaction is no longer dominant over the C_{60}-C_{60} interaction due to the small size of the Na^+ ion and thus there may be an interesting and nontrivial orientational ordering phase diagram in the temperature composition (of Na) plane.[5,6]

An exciting development having both fundamental and applied consequences was the discovery of superconductivity above 20 K in the doped fullerenes, M_3C_{60}, where M denotes a heavy monovalent metal such as K or Rb.[7–11] These superconducting doped fullerenes all have a fcc crystal structure[12,13] and the superconducting transition temperature T_c is found to be larger for those compounds with larger lattice constants.[10,11] Other doped systems such as M_4C_{60} which are body-centered tetragonal,[14] or M_6C_{60} which are body-centered cubic,[15] do not exhibit superconductivity in the temperature range investigated so far. One explanation to understand T_c for various dopants relates T_c to the density of states at the Fermi level, ρ_F.[16] Accordingly, there has been much interest in developing band-structure calculations for the M_3C_{60} systems.[17–19]

More recently, there has been a growing realization that there may be a close connection between the orientational state of M_3C_{60} and its superconducting properties. In a general way, it is obvious that the orientational configuration must affect the band structure, since the tight-binding matrix elements that describe hopping between adjacent C_{60} molecules can depend on their relative orientations. To the best of our knowledge Gelfand and Lu[20] were the first to give a band calculation which incorporates a dependence of the band structure on molecular orientations.

It would be desirable, therefore, to determine the orientational ground state of the C_{60} molecules in M_3C_{60}. From what we have said, it is clear that the orientational ground state will be determined by the combination of three types of energies: (1) the orientationally dependent part of the intermolecular interactions between neighboring C_{60} molecules, (2) the orientational potential energy of a C_{60} molecule in the Coulomb and short-range potential of its M neighbors, and (3) the orientationally dependent part of the band energy, mainly of the electrons transferred from the M^+ ions to the $C_{60}{}^{3-}$ ions. In what follows, we will refer to the sum of the first two types of interactions as the "direct interaction" and the last type as the "band interaction."

One simplifying feature of this problem is noteworthy. There is evidence that in the M_3C_{60} systems, the C_{60} molecules strongly preferentially occupy either one of the two "standard" orientations, shown in Fig. 1, in which each of the cubic (1,0,0) directions coincide with a twofold axis of the C_{60} molecule. The original x-ray-diffraction work of Stephens *et al.*[12] indicated a fcc lattice in which all molecules were equivalent. Stephens *et al.* interpreted

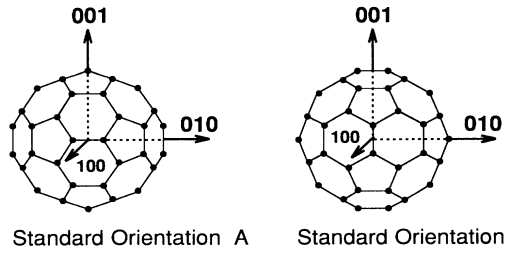

FIG. 1. The two standard orientations of a C_{60} molecule.

their data to indicate merohedral disorder in which each molecule had equal probability of occupying each of the two standard orientations shown in Fig. 1. Subsequent NMR work[21,22] showed a gradual evolution between a regime at temperatures well above T_0 in which the resonance line was severely motionally narrowed to a regime well below T_0 where the line became rather broad, presumably reflecting different orientational environments. As one might expect, T_0 is larger for M=Rb than for M=K, no doubt due to the larger size of the former ion. Presumably the motional narrowing can be interpreted as indicating a rapid (on the NMR time scale) motion of the molecule between the two standard orientations. At low temperature where transitions between the two standard orientations are frozen out, the system is probably an orientational glass, at least if one accepts the interpretation of Stephens *et al.* based on merohedral disorder. (It is possible that this model is too simple to explain the fine structure of the NMR line shapes.[23]) In any event, we will assume that the orientational state of each molecule can be taken to be one of the two standard orientations, the probability of intermediate orientations being small enough to neglect. This assumption is supported by experiment, as we have mentioned, and is also supported by estimates of the orientational potentials acting on a C_{60} molecule. Accordingly, when intermediate orientations are neglected, the orientational state of the system can be mapped exactly onto an Ising model in which one standard orientation corresponds to spin "up" and the other to spin "down." Actually, in the language of critical phenomena, we have not an Ising model, but rather a "soft spin" model with the molecules only preferring, rather than being strictly confined to, the two standard orientations. However, the qualitative behavior of the soft spin and Ising models is similar, and in particular, they have the same symmetry. Although the actual samples investigated so far may be orientational glasses, it would obviously be interesting to determine the equilibrium ground state and thermodynamic properties of this system.

In summary, in this report we will study the orientational ordering of C_{60} molecules in the equilibrium ground state of M_3C_{60}. In Sec. II, we first show that due to the short-range repulsive interactions between $C_{60}{}^{3-}$ and its M^+ neighbors, the system, is well described by a generalized Ising model. For this system, the effective interaction constant for sites i and j, $J_{ij} \equiv J(\mathbf{r}_{ij})$, couples neighbors at all separations, although it rapidly decays as r_{ij} becomes large. The direct contribution, discussed in Sec. II, to $J(\mathbf{r})$ is non-negligible only for nearest neighbors, for which case it is ferromagnetic. The band contribution to $J(\mathbf{r})$ is treated within two complementary approximations. In Sec. III we treat it exactly, but only for selected periodic structures with small unit cells. Then in Sec. IV we treat the system as a quenched random alloy, first by the virtual crystal approximation, and then by a perturbative approach to include configurational fluctuations beyond the virtual crystal approximation. Our conclusion from Secs. III and IV is that the ground state is antiferromagnetic. However, the detailed arrangement of sublattices depends on small energy differences which are hard to calculate reliably. A summary and further discussions are given in Sec. V.

II. INTERMOLECULAR INTERACTIONS IN M_3C_{60}

Experimentally, it has been well established that C_{60} molecules in M_3C_{60} are locked in one of two standard orientations as shown in Fig. 1.[12] This can be understood easily if we look at the interaction between a $C_{60}{}^{3-}$ molecule and its surrounding M^+ ions. The dominant term in this interaction is the short-range repulsive interactions between the M^+ alkali ions and the carbon atoms. We express this interaction, $V_{\rm int}$, by a 12-6 Lennard-Jones potential between the Ith C_{60} molecule and an M^+ ion as

$$V_{\rm int} = \sum_{i\in I} 4\epsilon\left[\left(\frac{\sigma}{r_{i,I}}\right)^{12} - \left(\frac{\sigma}{r_{i,I}}\right)^{6}\right], \qquad (1)$$

where $i \in I$ indicates that the sum is carried over atoms i in the molecule I. Here $r_{i,I}$ is the distance from the M^+ ion to the ith atom in molecule I. The parameters ϵ and σ are determined from the experimental lattice constant and compressibility.[24,25] For instance, for M =K, ϵ = 20.4 meV and σ = 3.083 Å. Figure 2 shows this short-range repulsive potential between a $C_{60}{}^{3-}$ and its

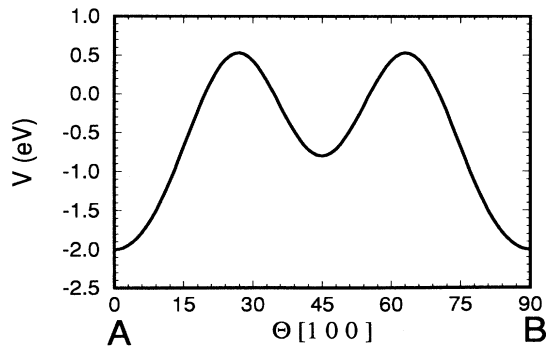

FIG. 2. The short-range repulsive potential energy for a C_{60} molecule located at (0,0,0) and interacting with its 14 surrounding K^+ ions as a function of rotation angle about the (100) axis going from the A setting to the B setting.

14 neighboring K^+ ions as the molecule rotates around the [100] axis from one standard orientation to the other. From this figure we see that two standard orientations A and B are well separated by a potential barrier of the order 2 eV. The fact that the potential barrier between two standard orientations is so large means that one may neglect orientations intermediate between the two standard orientations shown in Fig. 1.[26] Then the orientational interactions are the same as that of an Ising model in which spin up corresponds to one standard orientation and spin down to the other. Furthermore, in view of the cubic symmetry of the lattice, the interaction energy between a C_{60} molecule and the lattice of M ions is exactly the same when C_{60} is in orientation A as when it is in orientation B. [A reflection with respect to a (110) plane takes a C_{60} molecule from one setting to the other while leaving the positions of the alkali ions unchanged.] Accordingly, the "crystal" field acting on the C_{60} molecules due to the M^+ ions does not favor one standard orientation over the other, and therefore will not be considered any further.[27] Thus, we have only two types of energy terms that will determine the orientations of C_{60} molecules in the equilibrium ground state. The first one is the direct intermolecular interaction between neighboring C_{60} molecules. The second one, which will be discussed in Sec. III, is the orientationally dependent part of the band energy.

In this section we consider the direct interaction between C_{60} molecules. In our model the direct interaction Hamiltonian is

$$H_D = \sum_{\langle i,j \rangle} V_{ij}(\sigma_i, \sigma_j) \ , \tag{2}$$

where σ_i is the Ising variable ($+1$ for setting A and -1 for setting B), and $V_{ij}(\sigma_i, \sigma_j)$ is the interaction energy between C_{60} molecules at sites i and j, for settings corresponding to σ_i and σ_j. (When it is more appropriate we will label sites by their position vector $\mathbf{R} \equiv \mathbf{R}_i$ and write $\sigma_{\mathbf{R}}$ for σ_i.) Here $\langle i,j \rangle$ indicates that the sum runs over all pairs of nearest-neighboring molecules. From symmetry, V_{ij} does *not* depend on the indices i and j. This is because all pairs of nearest-neighboring C_{60} molecules are equivalent due to the symmetry of the fcc lattice. Thus we have only two values for V_{ij}, V_{AA} for a pair of molecules at setting AA (or BB) and V_{AB} for a pair at setting AB (or BA). Therefore, the Hamiltonian given above is

$$H_D = J_D \sum_{\langle i,j \rangle} \sigma_i \sigma_j + V_0 \ , \tag{3}$$

where V_0 is independent of the σ_i's and will therefore be dropped, and

$$J_D = (V_{AA} - V_{AB})/2 \tag{4}$$

and the symbol J_D emphasizes that it includes only the effect of direct interactions.

To estimate J_D we must rely on a model for the orientational-dependent part of the C_{60}-C_{60} interaction. We assume that for a pair of C_{60} molecules the potential consists of the interactions of neutral C_{60} molecules *plus* the additional Coulomb interaction due to the three additional electrons on each molecule. We first discuss the interaction between two neutral C_{60} molecules. Although it is customary to use Lennard-Jones atom-atom potentials for molecular solids, it was soon recognized that such a potential leads to an instability in the cubic structure,[28] in contradiction to the experimental result.[1] To remedy this defect, two improved potential models have been proposed.[29,30] In both cases the Lennard-Jones potential is supplemented by Coulomb interactions between effective charges introduced to describe the electronic charge density of a molecule. The observed $Pa3$ structure[31–34] of the orientationally ordered phase[1] is stabilized by adjusting these point charges. So far, many properties of solid C_{60} have been studied from these potential models.[35–37] Both potentials give almost the same phonon spectrum while the Lu *et al.* potential gives a somewhat higher libron spectrum than the Sprik *et al.* potential.[37] On the other hand, most recent experiments show that both phonons and librons have a higher frequency than these potential models predict,[38,39] indicating that potential models should be improved further. The other unsatisfactory feature of these potentials is that in order to stabilize $Pa3$ structure and give a reasonable transition temperature, they require unexpectedly large effective charges in the double and single bonds. Even worse, for the case of the Lu *et al.* potential, single bonds are positive relative to carbon sites, a situation which does not seem physical. To study this situation, in Ref. 40, Yildirim, Harris, Erwin, and Pederson (YHEP) calculated the multipoles of a C_{60} molecule from a quantum-mechanical (local-density approximation) charge density and compared the results to those resulting from the effective charges introduced in these models. Not surprisingly, YHEP found that the moments calculated quantum mechanically are one order of magnitude smaller than those implied by the bond-charge models. Thus, Coulomb interaction due to the anisotropic charge distribution of C_{60} molecules is much smaller than predicted so far. Accordingly, we do not think that the Coulomb terms in Lu *et al.* and Sprik *et al.* potentials really represent the Coulomb interactions due to the anisotropic charge distribution. However, we do not completely abandon these models because they may fortuitously include the effects of interactions such as the exchange and correlation energy or the interaction energy due to the charge overlap of the nearest-neighbor molecules.

In this paper we will use both the Lu *et al.* potential and the multipole expansion given in Ref. 40 in order to get estimates for the C_{60}-C_{60} interactions. We will not worry about the interactions between further than nearest-neighbor molecules even though we are dealing with long-range Coulomb interactions in an ionic solid. This simplification is due to the fact that orientational dependence of Madelung energy falls off with intermolecular distance as $1/R^{13}$, even if the molecules are not charge neutral.[41]

Thus, the direct interaction energy between two C_{60} molecules consists of two main terms: (1) the 12-6

TABLE I. The Lennard-Jones, with parameters $\epsilon = 2.964$ meV and $\sigma = 3.407$ Å taken from Ref. 30, and Coulomb potentials for the interaction of two nearest-neighbor molecules at orientations AA and AB for $a = 14.20$ Å.

Orientation of the interacting molecules	Lennard-Jones potential (eV)	Coulomb Potential (eV) Lu *et al.* pot. Ref. (30)		Multipole exp. Ref. (40)	
AA	−0.26291	−0.01589[a]	−0.00891[b]	0.00118[a]	−0.00106[b]
AB	−0.25923	0.06249[a]	0.03722[b]	0.00425[a]	0.00811[b]
J_D [c] $= (V_{AA} - V_{AB})/2$		−0.04103[a]	−0.02491[b]	−0.00338[a]	−0.00643[b]

[a]When $3e$ is distributed equally among carbon sites.
[b]When $3e$ is distributed equally among the pentagon centers.
[c]Note that J_D includes both the Lennard-Jones and the Coulomb potentials.

Lennard-Jones potential and (2) the total Coulomb interaction consisting of bond-bond, $3e$-$3e$, and $3e$-bond interactions. For the "bond charge density" we take the charge distribution of the neutral C_{60} molecule as given either by Lu, Li, and Martin[30] or by YHEP.[40] For the three transferred electrons we consider two quite different cases: (1) when $3e$ is equally distributed among carbon sites and (2) when $3e$ is equally distributed among the center of pentagons. The total Coulomb energy for the four possible scenarios is listed in Table I. For each scenario one obtains J_D via Eq. (4) when the Lennard-Jones energy is included. From this table we see that both potentials give a ferromagnetic ($J_D < 0$) interaction. Also note that the potential given by Lu, Li, and Martin predicts an energy difference between the two orientations which is larger by an order of magnitude than that obtained from the multipole expansion, which we use in this paper.

In conclusion, if we neglect the kinetic energy of the conduction electrons, the system will have a ground state where all C_{60} molecules are ordered in the same orientation with space group $Fm\bar{3}$. However, as we shall see in Sec. III, the kinetic energy of the band electrons must be taken into account.

III. KINETIC ENERGY OF THE CONDUCTION ELECTRONS

In Sec. II, we observed that the direct interactions between the charged C_{60} molecules in the M_3C_{60} phases favor the formation of an orientationally ordered phase with $Fm\bar{3}$ symmetry, i.e., a phase in which the molecules uniformly order in the A (or B) orientation on a fcc Bravais lattice. The failure to observe such an ordered phase in experiments[12] may be due to quenching this system into an orientational glass, where the energy barriers to reorientation are too large to allow equilibration to the $Fm\bar{3}$ phase on an accessible experimental time scale. It is also possible that various nonclassical interactions not considered in the model of Sec. II prevent ordering in this $Fm\bar{3}$ phase. In the following two sections we pursue this second point and consider more carefully the contributions to the total energy coming from the kinetic energy of the conduction electrons in this system. We find that these electronic contributions favor configurations with nearest-neighbor bonds between molecules with inequivalent orientations. In other words, the effective Ising interaction J_B^{NN} between nearest neighbors due to band interactions is antiferromagnetic. As we shall see, when this interaction is combined with that due to direct interactions, the total nearest-neighbor interaction is reduced, but is probably still antiferromagnetic. The total second-neighbor interaction is due almost exclusively to band interactions and is ferromagnetic. The consequences of these results will be explored in Sec. V.

Now we consider the kinetic energy of the conduction electrons. The conduction band in the alkali-metal-doped fullerenes is derived from an orbitally threefold-degenerate t_{1u} state of the isolated molecule. The hopping amplitude between neighboring sites i and j can thus be represented by a real 3×3 matrix, $t(\tau)$, describing the amplitude for hopping of an electron from an orbital in any of three possible polarizations at site $\mathbf{R}$ to any of the orbital polarizations on the neighboring site $\mathbf{R}+\tau$. Gelfand and Lu[20] have emphasized that both the amplitudes and phases of the matrix elements appearing in $t(\tau)$ depend sensitively on the relative orientations of the molecules on the two neighboring sites. As a consequence, a random distribution of orientations of the C_{60} molecules on the lattice is very effective for scattering electrons at the Fermi surface of the disordered doped solid. This orientational disorder leads to a substantial redistribution of spectral weight in the t_{1u}-derived conduction band, and we now consider this effect in more detail.

To describe the orientation dependence of the nearest-neighbor hopping amplitudes we follow the analysis of Ref. 20. In their formulation the band Hamiltonian for the three p-like symmetry orbitals of the conduction band can be written as

$$\mathcal{H}_B = \sum_{\mathbf{R},\tau}\sum_{\alpha,\beta} t_{\alpha,\beta}(\tau;\sigma_{\mathbf{R}},\sigma_{\mathbf{R}+\tau}) c^{\dagger}_{\mathbf{R},\alpha} c_{\mathbf{R}+\tau,\beta} \ , \qquad (5)$$

where α and β range over the symmetry labels ($1 \equiv x$, $2 \equiv y$, or $3 \equiv z$) of the t_{1u} conduction-band orbitals and $\sigma_{\mathbf{R}}$ are the Ising variable introduced previously to specify the orientation of the molecule $\mathbf{R}$. (Below, when convenient, we will use $c_{i,\alpha}$ to denote $c_{\mathbf{R}_i,\alpha}$.) Since the hopping matrices can assume four values depending on the four values of the pair of σ variables involved, we may write

$$t_{\alpha,\beta}(\tau;\sigma_{\mathbf{R}},\sigma_{\mathbf{R}+\tau}) = t^{(0)}_{\alpha,\beta}(\tau) + t^{(1)}_{\alpha,\beta}(\tau)\sigma_{\mathbf{R}} + t^{(2)}_{\alpha,\beta}(\tau)\sigma_{\mathbf{R}+\tau} + t^{(3)}_{\alpha,\beta}(\tau)\sigma_{\mathbf{R}}\sigma_{\mathbf{R}+\tau} \ . \qquad (6)$$

For $\tau = (a/2)(\hat{i}+\hat{j}) \equiv \tau_0$, we have

$$t^{(0)}(\tau_0) = t\begin{bmatrix} A & B & 0 \\ B & A & 0 \\ 0 & 0 & C \end{bmatrix} \quad t^{(1)}(\tau_0) = t\begin{bmatrix} X & Y & 0 \\ -Y & -X & 0 \\ 0 & 0 & 0 \end{bmatrix}, \tag{7}$$

$$t^{(2)}(\tau_0) = t\begin{bmatrix} X & -Y & 0 \\ Y & -X & 0 \\ 0 & 0 & 0 \end{bmatrix} \quad t^{(3)}(\tau_0) = t\begin{bmatrix} D & E & 0 \\ E & D & 0 \\ 0 & 0 & F \end{bmatrix}. \tag{8}$$

The form of these matrices follows from symmetry considerations: Using the reflection that takes z into $-z$, we see that the x–z, y–z, z–x, and z–y elements of the above matrices must vanish. The reflection that interchanges x and y also takes one standard orientation into the other, i.e., it reverses the signs of σ_i and σ_j, from which we may conclude that $t^{(1)}_{zz} = t^{(2)}_{zz} = 0$ and that $t^{(1)}$ and $t^{(2)}$ are antisymmetric and traceless. This reflection also forces $t^{(0)}$ and $t^{(3)}$ to be symmetric with $t^{(0)}_{xx} = t^{(0)}_{yy}$ and $t^{(3)}_{xx} = t^{(3)}_{yy}$. Finally, inversion about the center of the bond τ implies that $t^{(1)}_{xx} = t^{(2)}_{xx}$ and $t^{(1)}_{xy} = t^{(2)}_{yx}$. A detailed derivation given in Appendix A leads to Eqs. (7) and (8), where the constants, listed in Table II, are identified from Ref. 20.

For reference, we consider first the density of states calculated for the orientationally ordered structure (space group $Fm\bar{3}$). At zero (or effectively at low enough) temperature, all states with $E < E_F$ are occupied, where E_F is the Fermi energy fixed to give three electrons per C_{60} molecule. The Fermi surface in this model consists of two sheets in reciprocal space and agrees quite well with the Fermi surface structure found in the far more detailed local-density calculations.[18] As expected for a p-like band, the zone center is a threefold-degenerate local maximum in the dispersion relation, and the extrema in this band are obtained at the **X** point $\mathbf{k} = \frac{2\pi}{a}(100)$.

One way to study the dependence of the band energy on orientations would be to consider progressively larger unit cells, within which arbitrary choices of the two standard orientations were allowed. Since this procedure is not very appealing, we have contented ourselves with calculations for a conventional unit cell containing four molecules on their fcc lattice sites but having arbitrary orientations. There are only three inequivalent choices of standard orientations: (A_4), the orientationally ordered model considered above; (A_3B) a structure in which one molecule (at the origin) is in the B standard orientation; and the other three molecules are in the A standard orientation. This structure belongs to the cubic space group $Pm\bar{3}$.[2] In model (A_2B_2) molecules at (0,0,0) and $(1/2,1/2,0)$ are in orientation A and those at $(0,1/2,1/2)$ and $(1,2/0,1/2)$ are in orientation B. This structure is noncubic, of course, having the crystal symmetry D_{4h}. The A_3B model is "less disordered" than the A_2B_2 model, in the sense that one-half of the nearest-neighbor bonds in the A_3B model and two-thirds of the nearest-neighbor bonds of the A_2B_2 model connect sites with inequivalent orientations.

TABLE II. Values of the constants in Eqs. (7) and (8).

A	B	C	D	E	F	X	Y
0.01	0.38	−2.29	2.09	− 2.36	0.38	−0.63	− 0.49

The conduction-band densities of states calculated in the three models are shown in Fig. 3. Two effects are apparent. First, the overall bandwidth is slightly smaller for the two nonferromagnetic orientational configurations. More importantly, there is pronounced redistribution of spectral weight in the conduction band. This leads to a modest suppression of the density of states at the Fermi energy, and the emergence of a peak near $-10t$ in both nonferromagnetic models. This effect is also seen in the numerical work reported by Gelfand and Lu.[20] In calculations on cells containing 864 molecules with quenched orientational disorder, they obtain a very small change in the total density of states at the Fermi energy and a systematic shift of spectral weight to higher binding energy in the Fermi sea.

The filled conduction sea contributes a one electron energy

$$E_{\mathrm{KE}} = 2\sum_{n,\mathbf{k}} E_{n,\mathbf{k}} f_{n,\mathbf{k}} \tag{9}$$

to the effective orientational potential in this system,

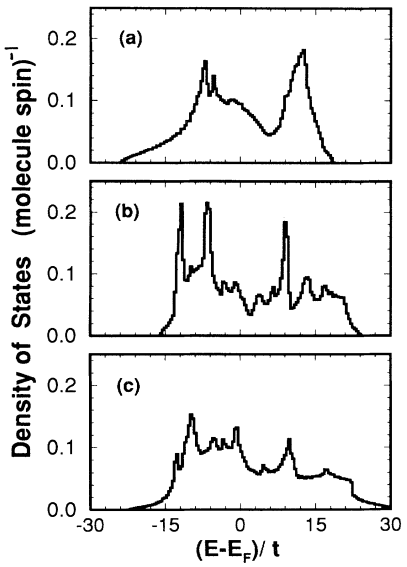

FIG. 3. Conduction-band densities of states (for fixed spin) obtained for (a) the A_4 structure with the four molecules in the same orientations; (b) the A_3B structure, with one of the molecules in the conventional cell flipped to the B orientation; (c) the A_2B_2 structure with two molecules flipped to the B orientation. To obtain three electrons per C_{60} molecule E_F is fixed to be $-0.75t$ for A_4, $-1.90t$ for A_3B, and $-2.05t$ for A_2B_2.

where n is a band label ($n = 1,2,3$) and $f_{n,\mathbf{k}}$ is the occupation number, which at low temperatures is 0 for $E_{n,\mathbf{k}} > E_F$ and 1 for $E_{n,\mathbf{k}} < E_F$. The factor 2 is for the sum over spin states. Carrying out the integral over the spectra shown in Fig. 3 yields the energies given in Table III.

The value of t in this table can be chosen to match the conduction-band width obtained from local-density calculations on these systems, leading to an estimate $t = 0.014$ eV for K_3C_{60}.[18] Thus the gain in kinetic energy (per cell relative to the A_4 structure) is $\Delta E(A_3B) = 0.165$ eV and $\Delta E(A_2B_2) = 0.134$ eV for the A_3B and A_2B_2 structures, respectively. Note that these results are inconsistent with a nearest-neighbor Ising model, which would give $\Delta E(A_2B_2)/\Delta E(A_3B) = \frac{4}{3}$. We note that the kinetic energy gained in the A_3B structure is 0.041 eV per molecule, which is somewhat larger than the direct interaction energy based on the multipole expansion, which favors the ferromagnetic A_4 arrangement. Thus, use of the multipole potential gives a total energy that favors a nonferromagnetic ground state. However, note that if the Coulomb interactions were described by the model of Ref. 30, they would dominate and the ground state would be ferromagnetic.

Since all potential models of Table I predict ferromagnetic J_D (i.e., J_D is negative) A_2B_2 structure has higher energy than A_3B structure no matter how small t is. Comparing energies of A_4 and A_3B, we find that A_3B has lower energy than A_4 if $t > -2.034J_D$. Using the calculated bandwidth in Ref. 19 and experimental lattice constant for Rb_2CsC_{60}, we get $t = 0.008$ eV and $J_D = -0.0017$ eV, which satisfy this inequality and guarantee that the ground state for this ternary is also nonferromagnetic. For other heavy alkali-metal (M=K, Rb , Cs) -doped binaries and ternaries, whose lattice constants fall between those of K_3C_{60} and Rb_2CsC_{60} the ground state is likewise expected to be nonferromagnetic.

We note that the A_2B_2 structure is, in fact, the ground state of the spin $\frac{1}{2}$ Ising model on the fcc lattice when the nearest-neighbor interaction is antiferromagnetic and the next-nearest-neighbor interaction is either zero[42] or ferromagnetic (F). However, the A_3B structure yields a lower kinetic energy for our interaction Hamiltonian, again emphasizing that the Hamiltonian is not equivalent to a nearest-neighbor antiferromagnetic (AF) Ising model.

TABLE III. Kinetic energies of the conduction electrons and the direct energies for orientational alloys of M_3C_{60}. The bottom panel shows the relative energies with respect to the A_4 structure. Here t sets the energy scale for the conduction bandwidth. For example, taking $t = 0.014$ eV one obtains a conduction bandwidth $W = 0.6$ eV, which is the result obtained from detailed calculations of the t_{1u} band using local-density theory for K_3C_{60}.[18]

Structure	Band energy per molecule	Direct energy per molecule
(A_4)	$-25.12t$	$6\ V_{AA}$
(A_3B)	$-28.07t$	$3V_{AA} + 3V_{AB}$
(A_2B_2)	$-27.52t$	$2V_{AA} + 4V_{AB}$
$(A_3B) - (A_4)$	$-2.95t$	$-6\ J_D$
$(A_2B_2) - (A_4)$	$-2.40t$	$-8\ J_D$

IV. THE EFFECTIVE ISING INTERACTION FROM BAND ENERGIES

The results of Sec. III demonstrate that the hopping amplitudes between nearest-neighbor molecules on the fcc lattice disfavors the orientationally ordered A_4 structure. In this section we provide further support for this idea by developing a perturbation theory for the one-electron kinetic energy near the orientationally disordered phase in terms of Ising order parameters for the orientational degrees of freedom.

We now consider the band energy as a function of the orientations of the molecules. In so doing, we should note that there are two different schemes one might use to calculate the alloy energy. In one case, one inserts the average hopping matrix element into the Hamiltonian. This approximation, known as the virtual crystal approximation, would be appropriate if the correlation time of the stochastic variable σ_i is short in comparison to the band frequencies, i.e., the band energies divided by $\hbar$. However, since we expect the correlation time for the σ_i to be even longer than the inverse of a libron frequency, this limit cannot apply. In the other limit, i.e., when the electronic bandwidth divided by $\hbar$ is large compared to the flipping frequency between molecular orientations, we should use a "quenched" average in which the ground-state energy $\frac{\langle |H| \rangle}{\langle | \rangle}$ is first calculated in an arbitrary configuration in order to obtain an effective potential for molecular orientations. Since the virtual crystal approximation is so simple to evaluate, we will include corrections towards the quenched average in a perturbative way.

To start, we study the orientationally disordered state within the virtual crystal approximation. That is we write Eq. (6) in the form

$$\mathcal{H}_B = \mathcal{H}_0 + \sum_i \mathcal{H}_1(i)\sigma_i + \tfrac{1}{2}\sum_{i,j} \mathcal{H}_2(i,j)\sigma_i\sigma_j \ . \qquad (10)$$

The virtual crystal approximation replaces σ_i with its average $[\sigma_i]$. In the absence of orientational order of any type, $[\sigma_i] = 0$. Thus the virtual crystal approximation for the disordered state is simply the band structure according to $\mathcal{H}_0$. The density of states obtained for the virtual crystal is shown in Fig. 4. The overall bandwidth is quite small ($\sim 18t$) and the spectral density exhibits a collapse of spectral weight towards the center of the band.

The difference between the quenched and annealed averages can be highlighted by a simple, although possibly extreme, model consisting of two molecules, where the hopping matrix element assumes positive or negative values, depending on the orientations of the two molecules:

$$\mathcal{H} = \sigma_1\sigma_2 t(c_1^\dagger c_2 + c_2^\dagger c_1) \ . \qquad (11)$$

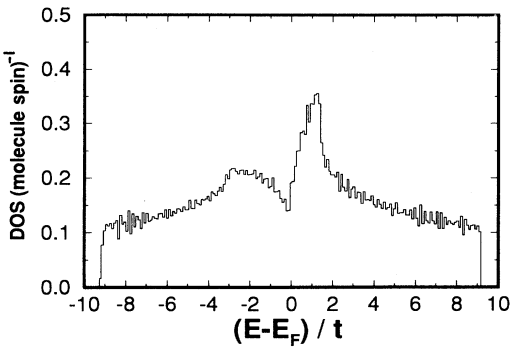

FIG. 4. As in Fig. 3 the conduction-band density of states obtained for the orientationally averaged virtual crystal Hamiltonian. E_F is fixed to be $0.335t$.

We discuss the ground-state energy when one orbital is occupied. In the virtual crystal approximation we replace $t\sigma_1\sigma_2$ with its average value, i.e., 0, or if there is partial, order with $\langle\sigma\rangle^2$. To get the quenched average, we note that the occupied orbital always has energy $-t$, so the quenched averaged energy is $-t$. As can be seen, the difference between quenched and annealed is that in the former case we allow the electronic wave functions to optimize themselves for each set of orientations of the molecules, whereas in the annealed average, the wave function does not readjust to each particular configuration, and therefore it has too high an energy. Thus we describe the system by an effective Hamiltonian that takes the form of a generalized Ising model: the Hamiltonian is

$$\begin{aligned}\mathcal{H}_{\text{eff}} &= J_D \sum_{\langle ij\rangle} \sigma_i\sigma_j + 2\sum_{\tau,\mathbf{k}} n_{\tau,\mathbf{k}} E_{\tau,\mathbf{k}}(\{\sigma_i\}) \\ &\equiv \tfrac{1}{2}\sum_{i,j} J_{ij}\sigma_i\sigma_j + \frac{1}{4!}\sum_{ijkl} J^{(4)}_{ijkl}\sigma_i\sigma_j\sigma_k\sigma_l + \dots \ , \end{aligned} \tag{12}$$

where, because of the symmetry between A and B orientations, there are no terms of odd order in the σ_i's. In this section we will not make any analysis of the four (or higher) spin interactions, although, as we shall see, they are non-negligible.

We now treat this Hamiltonian keeping only two spin interactions and using mean field theory, wherein we introduce order parameters $x_i \equiv \langle\sigma_i\rangle_T$, where $\langle\ \rangle_T$ denotes a thermal average. In terms of these order parameters, the mean-field free energy $\mathcal{F}$ is

$$\begin{aligned}\mathcal{F} = J_D \sum_{\langle ij\rangle} x_i x_j + 2\sum_{\tau,\mathbf{k}} n_{\tau,\mathbf{k}} E_{\tau,\mathbf{k}}(\{x_i\}) \\ + \tfrac{1}{2}k_B T \sum_i [(1+x_i)\ln(1+x_i) \\ + (1-x_i)\ln(1-x_i)] \ , \end{aligned} \tag{13}$$

where the last two lines represent the usual entropic contribution. As explained above, $E_{\tau\mathbf{k}}(\{x_i\})$ represents the quenched average over σ_i, whereas calculating this quantity by replacing σ_i with x_i *in the Hamiltonian* corresponds to a virtual crystal averaging over σ_i. At quadratic order in the x_i we have

$$\begin{aligned}\mathcal{F} &= \mathcal{F}_0 + \tfrac{1}{2}\sum_{i,j}[J_D\Gamma_{ij} + E_{i,j} + k_B T\delta_{i,j}]\, x_i x_j \\ &\equiv \mathcal{F}_0 + \tfrac{1}{2}\sum_{i,j}(\chi^{-1})_{ij} x_i x_j \\ &\equiv \mathcal{F}_0 + \tfrac{1}{2}\sum_{i,j}(k_B T\delta_{ij} + J_{ij}x_i x_j), \end{aligned} \tag{14}$$

where Γ_{ij} is unity if sites i and j are nearest neighbors and is zero otherwise and E_{ij} is the quadratic contribution due to band interactions. The last equality in Eq. (14) defines how we will obtain the effective exchange interactions from the free energy at quadratic order in the x's. In terms of Fourier transformed variables we write

$$\mathcal{F} = \mathcal{F}_0 + \tfrac{1}{2}\sum_{\mathbf{q}}[k_B T + J(\mathbf{q})]\, x(\mathbf{q})x(-\mathbf{q}) \ . \tag{15}$$

We now develop a general framework within which either annealed (virtual crystal) or quenched averages can be taken. General averages over orientations (i.e., over σ_i) will be denoted $[\sigma_i]_{\text{av}}$. Quenched and annealed averages will be denoted $[\cdots]_Q$ and $[\cdots]_{\text{VC}}$, respectively. To avoid notational confusion we emphasize that σ_i is an Ising variable, whereas its average $[\sigma_i]_{\text{av}} \equiv x_i$ is a Landau order parameter. Since σ_i assumes the values $+1$ and -1, we have the quenched averages

$$\begin{aligned}[(\sigma_i)^p]_Q = x_i \ , \quad p \text{ odd}, \\ = 1 \ , \quad p \text{ even} \ . \end{aligned} \tag{16}$$

To get the annealed averages, note that we replace σ_i with its average, so in effect

$$[(\sigma_i)^p]_{\text{VC}} = x_i^p \ . \tag{17}$$

As is well known, at linear order ($p = 1$) there is no difference between quenched and annealed averages.

With the above preamble, we now consider perturbation theory relative to the virtual crystal approximation for the disordered state. Thus we treat $\mathcal{H}_1$ and $\mathcal{H}_2$ perturbatively. Let $|0\rangle$ denote the ground state of $\mathcal{H}_0$, whose energy is E_0. Then, in first order perturbation theory the band energy is

$$\begin{aligned}E_B &= E_B^{(0)} + \sum_i \langle 0|\mathcal{H}_1(i)|0\rangle [\sigma_i]_{\text{av}} \\ &\quad + \tfrac{1}{2}\sum_{i,j}\langle 0|\mathcal{H}_2(i,j)|0\rangle [\sigma_i\sigma_j]_{\text{av}} \\ &\equiv E_B^{(0)} + E_1 \ , \end{aligned} \tag{18}$$

where $E_B^{(0)}$ is the band energy of the orientationally disordered state in the virtual crystal approximation.

Since i and j are distinct, the term E_1 is the same for both quenched and annealed averaging. It gives

$$E_B = E_B^{(0)} + \sum_i \langle 0|\mathcal{H}_1(i)|0\rangle x_i + \tfrac{1}{2}\sum_{i,j}\langle 0|\mathcal{H}_2(i,j)|0\rangle x_i x_j \ . \tag{19}$$

Since the term linear in x_i vanishes by symmetry, we have

$$E_1 = \tfrac{1}{2}\sum_{i,j}\langle 0|\mathcal{H}_2(i,j)|0\rangle x_i x_j \ . \tag{20}$$

Note that this term represents an effective nearest-neighbor coupling.

Consider now second order perturbation theory: $E_B = E_B^{(0)} + E_1 + E_2$, where E_2 has three types of terms:

$$E_{2,a} = -\sum_{i,j}\left\langle 0\left|\mathcal{H}_1(i)\frac{1}{\mathcal{E}}\mathcal{H}_1(j)\right|0\right\rangle [\sigma_i\sigma_j]_{\rm av}, \tag{21}$$

$$E_{2,b} = -\sum_{i,j,k}\left\langle 0\left|\mathcal{H}_1(i)\frac{1}{\mathcal{E}}\mathcal{H}_2(j,k)\right|0\right\rangle [\sigma_i\sigma_j\sigma_k]_{\rm av}, \tag{22}$$

$$E_{2,c} = -\tfrac{1}{4}\sum_{i,j,k,l}\left\langle 0\left|\mathcal{H}_2(i,j)\frac{1}{\mathcal{E}}\mathcal{H}_2(k,l)\right|0\right\rangle [\sigma_i\sigma_j\sigma_k\sigma_l]_{\rm av} \ , \tag{23}$$

where $\mathcal{E} \neq 0$ is the (positive) excitation energy of the intermediate state. Consider first, $E_{2,a}$. For the annealed average, we have

$$[\sigma_i\sigma_j]_{\rm VC} = x_i x_j \ , \tag{24}$$

whereas for quenched averaging Eq. (16) leads to

$$[\sigma_i\sigma_j]_Q = x_i x_j + \delta_{i,j}(1 - x_i^2) \ , \tag{25}$$

where $\delta_{i,j,k,\ldots}$ is zero unless all its indices are the same. An important consequence of this result is what we may call the "evenness" property: Averages of even (odd) powers of σ's yield even (odd) powers of the x's.

We have the quenched average result

$$E_{2,a} = -\sum_{i,j} x_i x_j \left\langle 0\left|\mathcal{H}_1(i)\frac{1}{\mathcal{E}}\mathcal{H}_1(j)\right|0\right\rangle + \sum_i x_i^2 \left\langle 0\left|\mathcal{H}_1(i)\frac{1}{\mathcal{E}}\mathcal{H}_1(i)\right|0\right\rangle + \text{const} \ , \tag{26}$$

where "const" indicates terms that do not depend on the x_i's. The virtual crystal result does not include the last two terms of this result. Note that the term involving x_i^2 gives rise to a wave-vector independent contribution to $\chi(\mathbf{q})^{-1}$. (Such a contribution does not influence the selection of the wave vector at which the instability occurs, which gives rise to orientational ordering.) Also note that the first term has further-than-nearest-neighbor interactions between the x_i's.

If we only wanted the virtual crystal result, we could stop here, because all further terms will include more than two powers of x_k. However, the quenched average quadratic in the x_i will have contributions from all orders in perturbation theory. Next, consider $E_{2,b}$. Due to the evenness property it gives no contributions quadratic in the x_i. Finally, we consider the term $E_{2,c}$, keeping only contributions quadratic in the x_i. Then, since, $i \neq j$ and $k \neq l$, we have in quadratic order in the x_i,

$$[\sigma_i\sigma_j\sigma_k\sigma_l]_Q \sim \delta_{i,k}x_j x_l + \delta_{i,l}x_j x_k + \delta_{j,k}x_i x_l + \delta_{j,l}x_i x_k - \delta_{i,k}\delta_{j,l}(x_i^2 + x_j^2) - \delta_{i,l}\delta_{j,k}(x_i^2 + x_j^2) \ , \tag{27}$$

which leads to the quenched average result for $E_{2,c}$,

$$E_{2,c} = -\sum_{i,j,k}\left\langle 0\left|\mathcal{H}_2(i,j)\frac{1}{\mathcal{E}}\mathcal{H}_2(j,k)\right|0\right\rangle x_i x_k(1-\delta_{i,k}) \ . \tag{28}$$

In summary, we have the following results. The virtual crystal result correct to quadratic order in the x_i's is

$$E_B^{\rm VC} = \tfrac{1}{2}\sum_{i,j}\langle 0\,|\mathcal{H}_2(i,j)|\,0\rangle\, x_i x_j - \sum_{i,j}\left\langle 0\left|\mathcal{H}_1(i)\frac{1}{\mathcal{E}}\mathcal{H}_1(j)\right|0\right\rangle x_i x_j \ . \tag{29}$$

Correct up to second order in perturbation theory the quenched average result is

$$E_B^Q = E_B^{\rm VC} + \sum_i\left\langle 0\left|\mathcal{H}_1(i)\frac{1}{\mathcal{E}}\mathcal{H}_1(i)\right|0\right\rangle x_i^2 - \sum_{i,j,k}\left\langle 0\left|\mathcal{H}_2(i,j)\frac{1}{\mathcal{E}}\mathcal{H}_2(j,k)\right|0\right\rangle x_i x_k(1-\delta_{i,k}). \tag{30}$$

This result is naturally expressed in terms of contribution to J_{ij} which we define as

$$J_{ij}^{(2)} = \langle 0\,|\mathcal{H}_2(i,j)|\,0\rangle, \tag{31}$$

$$J_{ij}^{(1,1)} = -2\left\langle 0\left|\mathcal{H}_1(i)\frac{1}{\mathcal{E}}\mathcal{H}_1(j)\right|0\right\rangle, \tag{32}$$

$$J_{ij}^{(2,2)} = -2\sum_k\left\langle 0\left|\mathcal{H}_2(i,k)\frac{1}{\mathcal{E}}\mathcal{H}_2(k,j)\right|0\right\rangle \ . \tag{33}$$

Thus, to the order we work,

$$J_{ij} = J_D\Gamma_{ij} + J_{ij}^{(2)} + \left[J_{ij}^{(1,1)} + J_{ij}^{(2,2)}\right](1-\delta_{ij}) \ . \tag{34}$$

Note that since $[\sigma_i^2]_Q = 1$, we will have $J_{ii} = 0$. To assess the convergence of the perturbative approach to the quenched average, it is convenient to identify the fluctuation term by which the quenched average differs from the virtual crystal average. We denote the contribution to J_{ij} from $E_B^Q - E_B^{\rm VC}$ in Eq. (30) by $J_{ij}^{\rm fluct}$, in which case we have

$$J_{ij}^{\rm fluct} = -J_{ij}^{(1,1)}\delta_{ij} + J_{ij}^{(2,2)}[1-\delta_{ij}] \ . \tag{35}$$

We now apply this formalism to the electronic Hamiltonian for the doped fullerene. We pass to a Fourier

representation of the ordering fields x_i, i.e.,

$$x_i = \sum_{\mathbf{q}} e^{i\mathbf{q}\cdot\mathbf{r}_i} x(\mathbf{q}) \tag{36}$$

and identify contributions to $J(\mathbf{q})$ from Eq. (15). From Eq. (6) we observe that there are two terms in the Hamiltonian which are linearly coupled to the Ising spin variables. It is useful to construct symmetric and antisymmetric combinations of these two potentials on each of the bonds in the network. Thus we define

$$t^{\pm}(\tau) = \left[t^{(1)}(\tau) \pm t^{(2)}(\tau)\right]/2 \,. \tag{37}$$

The perturbation can then be written in terms of two terms, one involving coupling to the total magnetization in the bond τ and the other involving coupling to the staggered magnetization in the bond τ. This formulation isolates the diagonal and off-diagonal components of $t^{(1)}$ and $t^{(2)}$. In this way we get $J^{(1,1)}(\mathbf{q}) = J^{+}(\mathbf{q}) + J^{-}(\mathbf{q})$ corresponding to the decomposition of Eq. (37), where

$$J^{\pm}(\mathbf{q}) = \frac{2}{N} \sum_{n,n',\lambda} |\langle n', \mathbf{q}+\lambda | V^{\pm} | n, \lambda \rangle|^2 \times \left[\frac{f_{n',\mathbf{q}+\lambda} - f_{n,\lambda}}{E_{n',\mathbf{q}+\lambda} - E_{n,\lambda}}\right], \tag{38}$$

where

$$V^{\pm} = \sum_{\alpha,\beta,\tau} [1 \pm e^{-i\mathbf{q}\cdot\tau}] t^{\pm}_{\alpha\beta}(\tau) c^{\dagger}_{\alpha}(\mathbf{q}+\lambda) c_{\beta}(\lambda) e^{-i\lambda\cdot\tau} \,. \tag{39}$$

Also, we have

$$J^{(2)}_{ij} = \left\langle 0 \left| \sum_{\alpha,\beta} t^{(3)}_{\alpha,\beta}(\tau_{i,j}) c^{\dagger}_{i,\alpha} c_{j\beta} \right| 0 \right\rangle \equiv \Gamma_{i,j} J_0 \,, \tag{40}$$

where Γ was defined in Eq. (14) and $\tau_{i,j} = \mathbf{R}_j - \mathbf{R}_i$. In Fourier space we write this contribution as

$$J^{(2)}(\mathbf{q}) = J_0 \Gamma(\mathbf{q}), \tag{41}$$

where

$$\Gamma(\mathbf{q}) = 4\left[\cos\left(\frac{q_x a}{2}\right)\cos\left(\frac{q_y a}{2}\right) + \cos\left(\frac{q_y a}{2}\right)\cos\left(\frac{q_z a}{2}\right) + \cos\left(\frac{q_z a}{2}\right)\cos\left(\frac{q_x a}{2}\right)\right] \tag{42}$$

is the structure factor for nearest neighbors on the fcc Bravais lattice. This can also be used to parametrize the direct electrostatic interaction obtained in Sec. II for which $J_D(\mathbf{q}) = J_D \Gamma(\mathbf{q})$, with $J_D < 0$, thus favoring the ferromagnetic, or orientationally ordered structure.

We now discuss the numerical implementation of the above analytic results. The various contributions to $J(\mathbf{q})$ are plotted along the symmetry directions of the fcc Brillouin zone in Fig. 5. The second order contributions $J^{-}(\mathbf{q})$ and $J^{+}(\mathbf{q})$, which are plotted in Fig. 5(a), favor orientational fluctuations at the **L** point and **X** point of the Brillouin zone, describing, respectively, orientationally modulated structures along the (111) and (001) crystal directions. As noted above, the direct contribution $J_D(\mathbf{q})$ provides a large negative potential at small momenta and thus favors the ferromagnetically ordered structure even if one takes the Coulomb interactions as given by the multipole expansion, using either column 3 or column 4 of Table I. However, this effect is offset by the bilinear electronic contribution $J^{(2)}(\mathbf{q}=0)$ which is also nearest neighbor but antiferromagnetic (i.e., $J_0 > 0$).

From Eq. (30) we also observe that the lowest order corrections to the virtual crystal theory are developed from terms which are second order in the scattering amplitudes. This correction, $J^{\text{fluct}}(\mathbf{q})$, is shown as the solid line in Fig. 5(a). The magnitude and wave-vector dependence of this correction is significant and it is comparable to the contributions from $J^{+}(\mathbf{q})$ and $J^{-}(\mathbf{q})$. However, the wave-vector dependence of $J^{\text{fluct}}(\mathbf{q})$ is such that it does not affect the wave-vector selection at the **X** point.

The full effective quadratic potential is then given by the solid line in Fig. 5(c). The resulting potential is op-

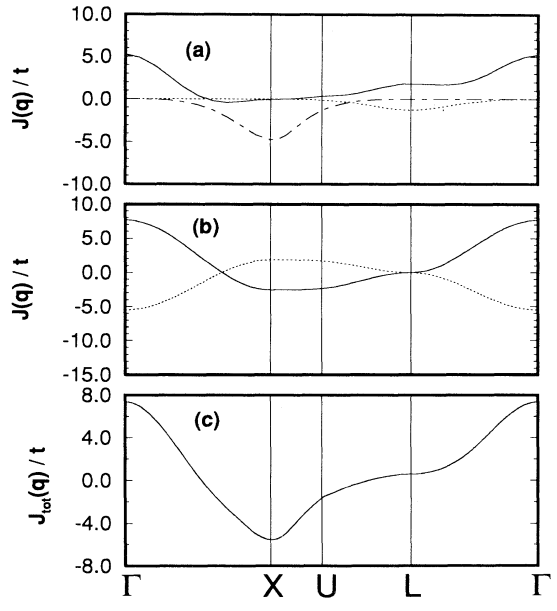

FIG. 5. The effective potentials $J(\mathbf{q})$ calculated for the virtual crystal reference state are plotted as a function of $\mathbf{q}$ along symmetry axes of the Brillouin zone. In the top panel (a) the second order perturbation corrections from $J^{-}(\mathbf{q})$ and $J^{+}(\mathbf{q})$ are plotted as the dotted curve and dot-dashed curve, respectively. The fluctuation correction $J^{\text{fluct}}(\mathbf{q})$ given in real-space representation in Eq. (30) is given by the solid curve. In the middle panel (b) the direct orientational interaction $J_D(\mathbf{q})$ (using J_D from column 4 of Table I) is plotted as the dotted curve, and the ground-state expectation value of the second-order potential $J^{(2)}(\mathbf{q})$ is plotted as solid curve. The sum of all these contributions is given in the lower panel (c). It is minimized at the **X** point and is not well described by a nearest-neighbor effective potential.

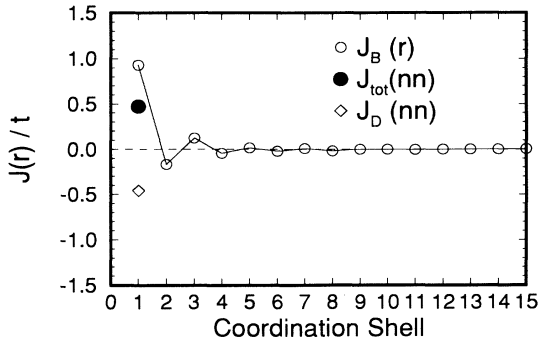

FIG. 6. The effective interaction $J(\mathbf{r})$ as a function of coordination shell. (A coordination shell includes all neighbors at a given distance. The angular dependence of J for fixed r is completely negligible.) The open circles are the contributions due to the band energy and the open diamond is that due to the direct interaction. The solid circle represents the total interaction. For further-than-nearest-neighbors, J_D is negligibly small and $J(r)$ coincides with the result due to the band energy.

timized at the **X** point, and this agrees with the ground-state studies of Sec. III, which favor the orientationally ordered alloy modulated at this wave vector. However, we also note that the effective Ising interaction J is no longer confined to nearest neighbors. As expected, this implies that the static response of the conduction sea is effective at mediating an indirect longer-range interaction between the fullerene sites.

It is also useful to give the results for the effective exchange interaction as a function of separation r between sites. In Eq. (29) it is clear that the first term gives rise to a nearest-neighbor interaction. The second term gives contributions at all separations and we determined it by Fourier transformation of the corresponding contribution to $J(\mathbf{q})$. Similarly, the first term in (30) is just what is needed to cancel the term at zero separation in $E_B^{\rm VC}$. The last term in Eq. (30) is a linear combination of interactions between neighbors up to fourth nearest neighbors. We determined the coefficients of this linear combination by fitting the data from Γ to X. We then checked that these coefficients did indeed reproduce the results for other high-symmetry directions. The results for $J(\mathbf{r})$ are given in Fig. 6.

V. DISCUSSIONS AND CONCLUSIONS

Here we discuss our results. We start by summarizing the conclusions from our ground-state calculations for periodic structures with small unit cells, namely the A_4, A_3B, and A_2B_2 structures. A comparison of the kinetic energies and direct interactions for these structures is given in Table III. From Table I we see that if we use the potential based on the bond charge models of Lu, Li, and Martin[30] or of Sprik, Cheng, and Klein,[29] we would obtain a ferromagnetic J for nearest neighbors of at least about 25 meV. Using a refined estimate of the multipole interactions (assuming charges distributed on the carbon sites and without any additional short-range interactions) we obtain an antiferromagnetic J for nearest neighbors of about 3 meV. Probably the best estimate lies somewhere between these two extremes.

Now we compare these results with those from the Landau expansion (Sec. IV). In the Landau expansion we looked for an instability from the disordered phase by calculating approximately the wave-vector-dependent Ising model susceptibility

$$\chi(\mathbf{q}) = [kT + J(\mathbf{q})]^{-1} \ . \tag{43}$$

The fundamental approximations we made here were (1) to use perturbation theory to incorporate configurational fluctuations that ought to be treated by a quenched configurational average, and (2) to neglect four and higher-spin interactions. Our results for $J(\mathbf{q})$, shown in Fig. 5, indicate an instability at the three X-point wave vectors of the paramagnetic Brillouin zone. It is reassuring that the crude approximation we used for the quenched average leads to an instability at the **X** point, consistent with our ground-state calculations. A general analysis of the Landau expansion of this instability is given in Appendix B. There it is shown that the sign of a particular fourth order anisotropy term in the free energy determines the nature of the ordered state. In particular, if this anisotropy is positive (as it is when the Hamiltonian contains only two-spin interactions), condensation into a single wave-vector state occurs. If this anisotropy is negative, then a so-called "triple-**q**" state[45] occurs with simultaneous condensation of all three equivalent X-point wave vectors. The former would naturally evolve (as the temperature is reduced) into an A_2B_2 state, whereas the latter would evolve into an A_3B state. Since according to the results given in Table III, the A_3B state is preferred, we believe that the relevant fourth order anisotropy is negative. When the Hamiltonian contains a four-spin interaction (scaled by $J^{(4)}$) involving a tetrahedron of nearest neighbors on a fcc lattice, the result of Appendix B is that we expect a triple-**q** state when

$$J^{(4)} > k_B T_c/24 \ , \tag{44}$$

where T_c is the transition temperature: $k_B T_c = -J(\mathbf{Q}_x)$, where $\mathbf{Q}_x$ is the wave vector at an **X** point. From Fig. 5, we see that $J(\mathbf{Q}_x) \approx -5t \approx -70$ meV, so that $J^{(4)} > 3$ meV is required to stabilize the A_3B structure found by our ground-state calculations.

As we have mentioned, our result for the first-neighbor pair interaction is not completely definitive because the direct orientational potential is rather uncertain. If, contrary to our expectation, this interaction is large and ferromagnetic the system is obviously ferromagnetic. Here we now give a brief discussion of the possible structures one might obtain for antiferromagnetic first-neighbor interactions but with various possible further neighbor or four-spin couplings. The most plausible such structures are shown in Fig. 7. Keeping only nearest and next-nearest pairwise interactions and a four-spin coupling, we have the model

$$\mathcal{H}_{\text{eff}} = \tfrac{1}{2}J_1 \sum_{\mathbf{r},\delta} \sigma_{\mathbf{r}}\sigma_{\mathbf{r}+\delta} + \tfrac{1}{2}J_2 \sum_{\mathbf{r},\delta'} \sigma_{\mathbf{r}}\sigma_{\mathbf{r}+\delta'} + J^{(4)} \sum_{T} \sigma_{T,1}\sigma_{T,2}\sigma_{T,3}\sigma_{T,4} \,, \tag{45}$$

where the δ is a nearest-neighbor vector, δ' is a second-nearest-neighbor vector, and in the last term, the sum over T is over tetrahedra of mutual nearest-neighboring spins, $\sigma_{T,i}$, for $i = 1,2,3,4$. By writing Eq. (45) we assume that the preference in our numerical work for the A_3B structure over the A_2B_2 structure is due to a four-spin term of the type written here. Then the energies per spin of the A_4, A_3B, and A_2B_2 structures are, respectively, $6J_1 + 3J_2 + 2J^{(4)}$, $3J_2 - 2J^{(4)}$, and $-2J_1 + 3J_2 + 2J^{(4)}$. It is easy to see that for $J^{(4)}$ negative, the A_4 structure is favored for negative J_1 and the A_2B_2 structure is favored for positive J_1. For $J^{(4)}$ positive the situation is as follows: For $J_1 > 2J^{(4)}$ the A_2B_2 structure has the minimum energy. For $-2J^{(4)} < -J_1 < 2J^{(4)}/3$, the A_3B structure is favored and, finally, for $J_1 < -2J^{(4)}/3$, the A_4 structure has the lowest energy. Our ground-state calculations indicate that these parameters should assume values so that the A_3B phase is stabilized at low T. But because of the small energy differences from our calculations, we cannot be certain about the exact values of the Ising interaction parameter $J^{(4)}$. Hence the various M_3C_{60} systems might be either the A_2B_2 or the A_3B structure shown in Fig. 7. Since these two structures have nearly the same energy, $J^{(4)}$ must be of order $J_1/2$ or larger and hence cannot be neglected.

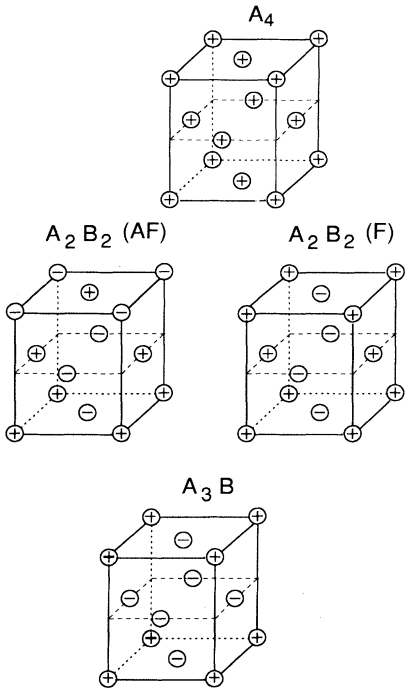

FIG. 7. Four possible arrangements of the sublattices. Top: the ferromagnetic A_4 ordering. Middle: two kinds of stacking of antiferromagnetic net planes for an antiferromagnetic Ising model on a fcc lattice. After the first horizontal plane is oriented, the second horizontal plane can choose either of two orientations which have exactly the same free energy by symmetry. The third horizontal plane will have a free energy which depends on whether it is in phase (F) or out of phase (AF) with the first plane. Thus in the F phase layer $(n+2)$ and layer (n) are parallel, whereas in the AF phase they are antiparallel. This type of breaking of degeneracy is similar to that in the body-centered tetragonal antiferromagnet (Ref. 44). Bottom: the A_3B structure that we estimate to be the ground state.

We should mention some difficulty in the unpublished work of Mazin *et al.* [Phys. Rev. Lett. **70**, 4142 (1993)]. A comparison of their results with those presented here is given elsewhere; Yildirim, Hong, Harris, and Mele (unpublished). In that work, the direct interaction is not considered at all. Their finding is that the first-neighbor interactions are antiferromagnetic and are dominant, in agreement with our band results plotted in Fig. 6. Then it is relevant to discuss the properties of the fcc Ising model with antiferromagnetic nearest-neighbor interactions as a function of the second-nearest-neighbor interaction. The results of Lebowitz, Phani, and Styer[42] show that in the absence of second-neighbor interactions, this system orders via a first-order transition at a temperature $T_0 \sim 1.8J$. At zero temperature this model has an infinite degeneracy in the way one layer is stacked on the next one. This stacking degeneracy is removed by thermal fluctuations, a phenomenon given the curious appellation "order from disorder."[43] This removal of degeneracy is equivalent to stating that thermal fluctuations give rise to an effective temperature-dependent second-neighbor-interaction $J_{\text{eff}}(T)$, which vanishes at $T = 0$, of course, but which is ferromagnetic at nonzero temperatures. As a result, one has the "second-nearest-neighbor ferromagnetic" configuration shown in Fig. 7. This ferromagnetic structure is just the A_2B_2 structure we have been considering. (It should be remarked that one still has an exact twofold degeneracy with respect to the stacking of the sublattice of odd-numbered layers with respect to the sublattice of even-numbered layers. However, this degeneracy has no important consequences.) This same removal of degeneracy happens for the body-centered tetragonal antiferromagnet.[44]

Since our determination of the sign of the second-neighbor interactions is not completely definitive, we briefly consider possible scenarios depending on the sign of J_2. Since we have already inferred a weak temperature-dependent effective second-neighbor interaction due to fluctuations, we expect that in the presence of weak second-neighbor interactions of strength J_2, the phase diagram is as shown in Fig. 8. At zero temperature, J_2, if nonzero, will resolve the stacking degeneracy. If J_2 is antiferromagnetic, it will compete with $J_{\text{eff}}(T)$, leading to a low-temperature phase boundary, as we show in Fig. 8. The two phases in Fig. 8 are depicted in Fig. 7. As in our calculations, Mazin *et al.* find that J_2 is ferromagnetic, in which case the ground state is predicted to be the second-nearest-neighbor ferromagnetic, which corresponds to A_2B_2 structure. This structure is noncubic, having D_{4h} symmetry. Presumably such a configuration of orientations would give rise to a cubic-to-tetragonal lattice distortion.

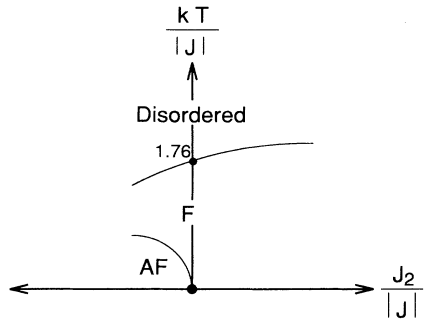

FIG. 8. Schematic phase diagram for the second-neighbor Ising antiferromagnet on a fcc lattice. For $J_2 = 0$ we use the results of Ref. 42. The point at $J_2 = 0$ at $T = 0$ is a special degeneracy point where all stackings of planes have degenerate energy. This degeneracy is resolved when either $T \neq 0$ or $J_2 \neq 0$. The resulting competition between these two parameters leads to the phase diagram shown here. The states labeled F and AF are depicted in Fig. 7.

Now we consider the experimental consequences of these results. First of all, the energy barrier between the two standard orientations is quite large. Experimentally, NMR spin-lattice-relaxation studies indicate a barrier of about 0.5 eV. Orientational potentials such as we use give a barrier of similar height. In pure C_{60} the analogous barrier is found to be about 275 meV and the Lu, Li, and Martin potential reproduces this estimate. From these data Lu, Li, and Martin estimate a freezing temperature, below which thermal activation over the barrier ceases, of about 90 K, in very good agreement with experimental data. Here, we would expect an analogous freezing temperature to be about twice as large, say, 175 K. Thus, these barriers are much larger than the energy differences between different Ising configurations, which we have just estimated to be of order 10–20 meV, depending on which potential is used. So, it seems likely that as the temperature is lowered, dynamic freezing will occur before orientational ordering. Such a conclusion is consistent with the model of merohedral disorder proposed by Stephens *et al.*[12] However, it remains to be checked whether or not allowing samples to equilibrate for very long times leads to behavior which might be identified as being closer to equilibrium.

Finally, we mention some consequences of a tetragonal distortion which, at least in principle, is the signature of the A_2B_2 structure. In the presence of such a distortion, the (k,k,k) powder diffraction peaks will remain sharp, whereas the other peaks, say $(k,0,0)$ will be split, or at least be broadened. [In contrast, a trigonal distortion would broaden the (k,k,k) peaks but leave $(k,0,0)$ peaks sharp.] Indeed, the experiments of Zhu *et al.*[13] show results consistent with a tetragonal distortion, but they interpreted their results as being due to stacking faults.

We may summarize our conclusions as follows.

(1) The direct interactions (Coulomb, Lennard-Jones, etc.) favor having all molecules in the same standard orientation, whereas the band energy favors having nearest neighbors in different standard orientations. If the direct interactions are taken from the multipole expansion, the band energy is somewhat larger. If the potential of Lu, Li, and Martin is used, the direct interaction is clearly dominant and all molecules assume the same standard orientations.

(2) Our calculations, although not conclusive, suggest that the A_3B state (shown in Fig. 7) is the ground state.

(3) It is significant that the energy a molecule can gain by making a transition from one standard orientation to another is smaller by a factor of about 50 than the height of the barrier between these two configurations. Consequently, the temperature at which one expects orientational ordering is less than the temperature at which hopping over the barrier is frozen out. Thus, orientational ordering is unlikely to be realized on experimental time scales. In that case, the model of an orientational glass with merohedral disorder is appropriate at temperatures below about 200 K.

(4) A study of the equilibration of these systems might also be useful. It would be interesting to see if the libron spectrum is time dependent, as one would expect, if the molecular orientations were slowly relaxing towards equilibrium. In a similar vein, it would be interesting to see if inelastic neutron scattering could prove the existence of anomalous libron-phonon interactions, which the orientationally dependent band energies would imply.

ACKNOWLEDGMENTS

This work was supported in part by the National Science Foundation under Grant No. DMR88-19885. A.B.H and T.Y. were supported in part by the NSF under Grant No. NSF-91-22784. S.H. and E.J.M. were supported in part by DOE Contract No. 91ER45118. Some of the computations were supported by a grant from the Research Foundation of the University of Pennsylvania.

APPENDIX A: HOPPING HAMILTONIAN

In this Appendix we discuss how the constants were fixed in the hopping Hamiltonian of Eq. (5). The intermolecular hopping matrix elements depend on the orientation of the molecules and on the polarization indices of the t_{1u} electronic states involved. Their evaluation was done by Gelfand and Lu.[20] Although we agree with their evaluation, Ref. 20 does not specify the matrix elements completely. We provide a complete specification below.

The calculations were carried out in the so-called radial atomic orbital approximation in which each carbon is assigned a p_r orbital, where r indicates polarization in the radial direction. The intermolecular hopping amplitude between a radial atomic orbital at site i of a molecule centered at $\mathbf{R}$ and one on site j of a molecule centered at $\mathbf{R}'$ is then expressed as

$$\begin{aligned}\mathbf{V}(\mathbf{r}_i,\mathbf{R};\mathbf{r}_j,\mathbf{R}') &= \langle \mathbf{r}_i,\mathbf{R}|\mathcal{H}|\mathbf{r}_j,\mathbf{R}'\rangle \\ &= a(r_{ij})\mathbf{r}_i\cdot\mathbf{r}_j \\ &\quad +b(r_{ij})(\mathbf{r}_i\cdot\mathbf{r}_{ij})(\mathbf{r}_j\cdot\mathbf{r}_{ij})\,, \qquad \text{(A1)}\end{aligned}$$

where $a(r)$ and $b(r)$ were determined as discussed in Ref. 20. Here, $\mathbf{r}_i$ is the position of site i relative to the

center of the molecule and lies in the radial direction at site i and $\mathbf{r}_{ij} = \mathbf{r}_i - \mathbf{r}_j + \mathbf{R} - \mathbf{R}'$. When $\mathbf{R}$ and $\mathbf{R}'$ are nearest-neighboring molecules, the 60×60 array of coefficients, $\mathbf{V}$, is dominated by a relatively small number of interactions between atomic sites for which r_{ij} is close to the minimum possible value. To discuss hopping between the lowest unoccupied molecular orbitals (LUMO's) of neutral C_{60} molecules on a fcc lattice (i.e., to get the kinetic energy of the half-filled conduction band of M_3C_{60}) we must project the above matrix $\mathbf{V}$ onto the appropriate single-particle states found by diagonalizing the *intramolecular* hopping Hamiltonian on a single C_{60} molecule. This was done in Ref. 20 and for a molecule at $\mathbf{R}$ gave the three t_{1u} LUMO's as

$$|\alpha, \mathbf{R}\rangle = \sum_{\mathbf{r}} \mathbf{g}_\alpha(\mathbf{r}) |\mathbf{r}, \mathbf{R}\rangle \ . \tag{A2}$$

We will discuss the symmetry label α in detail in a moment. Now the real symmetric matrix $\mathbf{V}$ of Eq. (A1) within the LUMO subspace is given in terms of the expansion coefficients of Eq. (A2) as

$$V(\alpha, \beta; \mathbf{R}, \mathbf{R}') = \sum_{\mathbf{r},\mathbf{s}} \mathbf{g}_\alpha(\mathbf{r})^* \mathbf{g}_\beta(\mathbf{s}) \mathbf{V}(\mathbf{r}, \mathbf{R}; \mathbf{s}, \mathbf{R}') \ . \tag{A3}$$

We need to analyze this result when the molecules are restricted to being in either standard orientation A or standard orientation B of Fig. 1. Accordingly, we denote the left-hand side of Eq. (A3) as the matrix $\mathbf{V}(X, Y; \tau)$ when the molecule at $\mathbf{R}$ is in orientation X and that at $\mathbf{R}'$ is in Y and $\tau = \mathbf{R} - \mathbf{R}'$. For standard orientation A, Eq. (A2) will produce an x-like t_{1u} function which is an odd function of x and an even function of y and z. For this function we write

$$|x, \mathbf{R}; A\rangle = \sum_{\mathbf{r} \in A} G_x(\mathbf{r}) |\mathbf{r}, \mathbf{R}\rangle \ , \tag{A4}$$

where $\mathbf{r} \in A$ indicates that $\mathbf{r}$ is summed over all sites when the molecule is in standard orientation A. [To understand the symmetry of this function it is helpful to imagine that $G_x(\mathbf{r}) = x(Ay^2 + Bz^2)$, with $A \neq B$.] The other partners in this t_{1u} representation can be expressed as

$$\begin{aligned} |y, \mathbf{R}; A\rangle &= \sum_{\mathbf{r} \in A} G_x(\mathbf{r}) |\mathcal{R}\mathbf{r}, \mathbf{R}\rangle = \sum_{\mathbf{r} \in A} G_x(\mathcal{R}^{-1}\mathbf{r}) |\mathbf{r}, \mathbf{R}\rangle \\ &\equiv \sum_{\mathbf{r} \in A} G_y(\mathbf{r}) |\mathbf{r}, \mathbf{R}\rangle \end{aligned} \tag{A5}$$

and

$$\begin{aligned} |z, \mathbf{R}; A\rangle &= \sum_{\mathbf{r} \in A} G_x(\mathbf{r}) |\mathcal{R}^2\mathbf{r}, \mathbf{R}\rangle = \sum_{\mathbf{r} \in A} G_x(\mathcal{R}^{-2}\mathbf{r}) |\mathbf{r}, \mathbf{R}\rangle \\ &\equiv \sum_{\mathbf{r} \in A} G_z(\mathbf{r}) |\mathbf{r}, \mathbf{R}\rangle \ , \end{aligned} \tag{A6}$$

where $\mathcal{R}$ is a rotation operator: $\mathcal{R}(x\hat{\mathbf{i}} + y\hat{\mathbf{j}} + z\hat{\mathbf{k}}) = z\hat{\mathbf{i}} + x\hat{\mathbf{j}} + y\hat{\mathbf{k}}$. The states $|y\rangle$ and $|z\rangle$ are odd functions of y and z, respectively.

It is now necessary to specify the wave functions for standard orientation B, in terms of those defined above for standard orientation A. There are two obvious ways to do this. One way, which we use in this paper, is to define a state $|x, \mathbf{R}; B\rangle$ such that this state is an odd function of x, where the coordinate axes x are the same on all molecules. In this approach one notes that standard orientation B is obtained from standard orientation A by a reflection σ about $x = y$. [Thus $\sigma(x\hat{\mathbf{i}} + y\hat{\mathbf{j}} + z\hat{\mathbf{k}}) = y\hat{\mathbf{i}} + x\hat{\mathbf{j}} + z\hat{\mathbf{k}}$.] Then we write

$$|y, \mathbf{R}; B\rangle = \sum_{\mathbf{r} \in A} G_x(\mathbf{r}) |\sigma\mathbf{r}, \mathbf{R}\rangle = \sum_{\mathbf{r} \in B} G_x(\sigma\mathbf{r}) |\mathbf{r}, \mathbf{R}\rangle \ . \tag{A7}$$

Likewise,

$$\begin{aligned} |x, \mathbf{R}; B\rangle &= \sum_{\mathbf{r} \in A} G_x(\mathbf{r}) |\sigma\mathcal{R}\mathbf{r}, \mathbf{R}\rangle \\ &= \sum_{\mathbf{r} \in B} G_x(\mathcal{R}^{-1}\sigma\mathbf{r}) |\mathbf{r}, \mathbf{R}\rangle \\ &= \sum_{\mathbf{r} \in B} G_y(\sigma\mathbf{r}) |\mathbf{r}, \mathbf{R}\rangle \ , \end{aligned} \tag{A8}$$

$$\begin{aligned} |z, \mathbf{R}; B\rangle &= \sum_{\mathbf{r} \in A} G_x(\mathbf{r}) |\sigma\mathcal{R}^2\mathbf{r}, \mathbf{R}\rangle = \sum_{\mathbf{r} \in B} G_x(\mathcal{R}^{-2}\sigma\mathbf{r}) |\mathbf{r}, \mathbf{R}\rangle \\ &= \sum_{\mathbf{r} \in B} G_z(\sigma\mathbf{r}) |\mathbf{r}, \mathbf{R}\rangle \ . \end{aligned} \tag{A9}$$

The other approach is that used by Gelfand and Lu in which they refer functions on different molecules to different local coordinates. That is, to get wave functions for standard orientation B, they rotate the wave functions by 90° about the z axis.[46]

Thus, for instance, indicating their functions by subscripts "GL" we write

$$\begin{aligned} |x, \mathbf{R}; B\rangle_{\mathrm{GL}} &= \sum_{\mathbf{r} \in A} G_x(-y, x, z) |\mathbf{r}, \mathbf{R}\rangle \\ &= -\sum_{\mathbf{r} \in A} G_x(y, x, z) |\mathbf{r}, \mathbf{R}\rangle \\ &= -|y, \mathbf{R}; B\rangle \end{aligned} \tag{A10}$$

$$\begin{aligned} |y, \mathbf{R}; B\rangle_{\mathrm{GL}} &= \sum_{\mathbf{r} \in A} G_y(-y, x, z) |\mathbf{r}, \mathbf{R}\rangle \\ &= \sum_{\mathbf{r} \in A} G_y(y, x, z) |\mathbf{r}, \mathbf{R}\rangle \\ &= |x, \mathbf{R}; B\rangle \ , \end{aligned} \tag{A11}$$

and

$$\begin{aligned} |z, \mathbf{R}; B\rangle_{\mathrm{GL}} &= \sum_{\mathbf{r} \in A} G_z(-y, x, z) |\mathbf{r}, \mathbf{R}\rangle \\ &= \sum_{\mathbf{r} \in A} G_z(y, x, z) |\mathbf{r}, \mathbf{R}\rangle \\ &= |z, \mathbf{R}; B\rangle \ . \end{aligned} \tag{A12}$$

The wave functions given in Eqs. (A4)–(A6) for the "A" orientation are the same as in Ref. 20.

The matrix $\mathbf{V}(X,Y;\tau_0)$ in the basis used by GL for $\tau_0=(a/2)(1,1,0)$ is[20]

$$\mathbf{V}(A,A;\tau_0)=t\begin{bmatrix}0.83&-1.98&0\\-1.98&3.36&0\\0&0&-1.91\end{bmatrix}, \tag{A13}$$

$$\mathbf{V}(A,B;\tau_0)^{\mathrm{GL}}=t\begin{bmatrix}1.75&2.08&0\\-2.08&-3.71&0\\0&0&-2.67\end{bmatrix}, \tag{A14}$$

where the superscript "GL" emphasizes that this is the result in the GL basis. Also the scale factor t determines the width of the conduction band. In view of Eqs. (A10)–(A12) we have, in our representation,

$$\begin{aligned}\mathbf{V}(A,B;\tau_0)&=\mathbf{V}(A,B;\tau_0)^{\mathrm{GL}}\begin{bmatrix}0&1&0\\-1&0&0\\0&0&1\end{bmatrix}\\&=t\begin{bmatrix}-2.08&1.75&0\\3.71&-2.08&0\\0&0&-2.67\end{bmatrix}.\end{aligned} \tag{A15}$$

We note that $\mathbf{V}(A,B;\tau_0)=\mathbf{V}(A,B;-\tau_0)$, which implies that $\mathbf{V}(B,A;\tau_0)=\mathbf{V}^T(A,B;\tau_0)$. Finally, we can relate $\mathbf{V}(B,B;\tau_0)$ to $\mathbf{V}(A,A;\tau_0)$ by using Eqs. (A7)–(A9) to relate the wave functions for orientation B to those for orientation A. In this analysis one uses the fact that

$$\mathbf{V}(\sigma\mathbf{r},0;\sigma\mathbf{s};\tau_0)=\mathbf{V}(\sigma\mathbf{r},0;\sigma\mathbf{s};\sigma\tau_0)=\mathbf{V}(\mathbf{r},0;\mathbf{s};\tau_0)\ . \tag{A16}$$

The conclusion is that

$$\begin{aligned}\mathbf{V}(B,B;\tau_0)&=\begin{bmatrix}0&1&0\\1&0&0\\0&0&1\end{bmatrix}\mathbf{V}(A,A;\tau_0)\begin{bmatrix}0&1&0\\1&0&0\\0&0&1\end{bmatrix}\\&=t\begin{bmatrix}3.36&-1.98&0\\-1.98&0.83&0\\0&0&-1.91\end{bmatrix}.\end{aligned} \tag{A17}$$

With the four matrices $\mathbf{V}(X,Y;\tau_0)$ the identification of the matrices in Eq. (6) is straightforward. We have

$$\begin{bmatrix}\mathbf{t}^{(0)}(\tau_0)\\\mathbf{t}^{(1)}(\tau_0)\\\mathbf{t}^{(2)}(\tau_0)\\\mathbf{t}^{(3)}(\tau_0)\end{bmatrix}=\frac{1}{4}\begin{bmatrix}1&1&1&1\\1&1&-1&-1\\1&-1&1&-1\\1&-1&-1&1\end{bmatrix}\begin{bmatrix}\mathbf{V}(A,A;\tau_0)\\\mathbf{V}(A,B;\tau_0)\\\mathbf{V}(B,A;\tau_0)\\\mathbf{V}(B,B;\tau_0)\end{bmatrix}. \tag{A18}$$

Using this relation we obtain the results of Eqs. (7) and (8), where the constants are listed in Table II.

APPENDIX B: LANDAU EXPANSION

In this Appendix we discuss the role of four-spin interactions in the Landau expansion. We therefore treat the Hamiltonian

$$\mathcal{H}=\tfrac{1}{2}\sum_{\mathbf{r},\mathbf{R}}J(\mathbf{r})S_z(\mathbf{R})S_z(\mathbf{R}+\mathbf{r})+J^{(4)}\sum_{\mathrm{T}}\prod_{\mathbf{r}\in\mathrm{T}}S_z(\mathbf{r})\ , \tag{B1}$$

where S_z assumes the values $+1$ and -1 and the last sum is over tetrahedra of nearest-neighboring sites. We introduce the mean-field approximation for the density matrix $\rho=\prod_{\mathbf{r}}\rho(\mathbf{r})$, where

$$\rho(\mathbf{r})=\tfrac{1}{2}\left[1+\sigma(\mathbf{r})S_z(\mathbf{r})\right] \tag{B2}$$

in terms of local order parameters $\sigma(\mathbf{r})$. For $J^{(4)}=0$ one has the standard result for the free energy, $\mathcal{F}$:

$$\begin{aligned}\mathcal{F}\equiv\mathrm{Tr}\left[\rho\mathcal{H}+k_BT\rho\ln\rho\right]&=\tfrac{1}{2}\sum_{\mathbf{q}}\chi(\mathbf{q})^{-1}\sigma(\mathbf{q})\sigma(-\mathbf{q})\\&\quad+\frac{k_BT}{12}\sum_{\mathbf{r}}\sigma(\mathbf{r})^4+O(\sigma^6)\ ,\end{aligned} \tag{B3}$$

where $\chi(\mathbf{q})=[k_BT+J(\mathbf{q})]^{-1}$ and we have the Fourier transforms

$$J(\mathbf{q})=\sum_{\mathbf{r}}J(\mathbf{r})e^{i\mathbf{q}\cdot\mathbf{r}}\ ;\qquad \sigma(\mathbf{q})=\frac{1}{\sqrt{N}}\sum_{\mathbf{r}}\sigma(\mathbf{r})e^{i\mathbf{q}\cdot\mathbf{r}}\ . \tag{B4}$$

Here we only keep the components of the **X**-point wave vectors $\mathbf{Q_x}\equiv 2\pi(1,0,0)/a$, $\mathbf{Q_y}\equiv 2\pi(0,1,0)/a$, and $\mathbf{Q_z}\equiv 2\pi(0,0,1)/a$, in which case we write

$$\sigma(\mathbf{r})=\frac{1}{\sqrt{N}}\left[e^{i\mathbf{Q_x}\cdot\mathbf{r}}\sigma_x+e^{i\mathbf{Q_y}\cdot\mathbf{r}}\sigma_y+e^{i\mathbf{Q_z}\cdot\mathbf{r}}\sigma_z\right]\ , \tag{B5}$$

where $\sigma_x=\sigma(Q_x)$, $\sigma_y=\sigma(Q_y)$, and $\sigma_z=\sigma(Q_z)$.

The fourth-order term in Eq. (B3) is

$$\frac{k_BT}{12}\sum_{\mathbf{r}}\sigma(\mathbf{r})^4=\frac{k_BT}{12N}\left[(\sigma_x^2+\sigma_y^2+\sigma_z^2)^2+4f_4\right]\ , \tag{B6}$$

where $f_4\equiv\sigma_x^2\sigma_y^2+\sigma_y^2\sigma_z^2+\sigma_x^2\sigma_z^2$. Note that the coefficient of the anisotropic term (involving f_4) is positive. This ensures that for two-spin interactions the ordering involves condensation of only one order parameter, i.e., either σ_x, σ_y, or σ_z. For such a model simultaneous condensation of the three **X**-point wave vectors does not occur.

Now we consider the case when $J^{(4)}$ is nonzero. The sites of a tetrahedron of nearest-neighboring sites ($i=1,4$) can be written as

$$\mathbf{R}+\mathbf{s}+\delta_i\ , \tag{B7}$$

where $\mathbf{R}$ is a Bravais lattice vector of the fcc lattice, $\mathbf{s}=(a/4)(1,1,1)$ and

$$\begin{aligned}&\delta_1=(a/4)(-1,-1,-1)\ ,\qquad \delta_2=(a/4)(1,1,-1)\ ,\\&\delta_3=(a/4)(1,-1,1)\ ,\qquad \delta_4=(a/4)(-1,1,1)\ .\end{aligned} \tag{B8}$$

There are also tetrahedra corresponding to reversing the signs of s and all the δ's. We call the former type "up"

tetrahedra and the latter as "down" tetrahedra. Then δF_4, the contribution to the free energy proportional to $J^{(4)}$, is

$$\delta F_4 = J^{(4)} \sum_{\mathbf{R}} \left[\prod_{\mathbf{i}} \sigma(\mathbf{R}+\mathbf{s}+\delta_i) + \prod_{\mathbf{i}} \sigma(\mathbf{R}-\mathbf{s}-\delta_i) \right] . \tag{B9}$$

We now use Eq. (B5) for $\sigma(\mathbf{r})$ to write the above result as

$$\begin{aligned} \delta F_4 &= \frac{2J^{(4)}}{N} \left[\sigma_x^4 + \sigma_y^4 + \sigma_z^4 - 2f_4 \right] \\ &= \frac{2J^{(4)}}{N} \left[(\sigma_x^2 + \sigma_y^2 + \sigma_z^2)^2 - 4f_4 \right] . \end{aligned} \tag{B10}$$

Then the Landau expansion for $J^{(4)} \neq 0$ is

$$\begin{aligned} \mathcal{F} = \tfrac{1}{2}\chi^{-1}(\mathbf{q})\sigma^2 + \left(\frac{k_B T}{12N} + \frac{2J^{(4)}}{N} \right) \sigma^4 \\ + f_4 \left(\frac{k_B T}{3N} - \frac{8J^{(4)}}{N} \right) + O(\sigma^6) , \end{aligned} \tag{B11}$$

where $\sigma^2 = \sigma_x^2 + \sigma_y^2 + \sigma_z^2$.

Note that if $J^{(4)}$ is positive and large enough, the coefficient of f_4 becomes negative, in which case we get simultaneous condensation of all three wave vectors.

[1] P. A. Heiney, J. E. Fischer, A. R. McGhie, W. J. Romanow, A. M. Denenstien, J. P. McCauley, Jr., A. N. Smith III, and D. E. Cox, Phys. Rev. Lett. **66**, 2911 (1991).

[2] A. B. Harris and R. Sachidanandam, Phys. Rev. B **46**, 4944 (1992).

[3] W. I. F. David, R. M. Ibberson, T. J. S. Dennis, J. P. Hare, and K. Prassides, Europhys. Lett. **18**, 225 (1992).

[4] G. B. M. Vaughan, P. A. Heiney, D. E. Cox, J. E. Fischer, A. R. McGhie, A. L. Smith, R. M. Strongin, M. A. Cichy, and A. B. Smith, III, Chem. Phys. (to be published).

[5] M. J. Rosseinsky, D. W. Murphy, R. M. Fleming, R. Tycko, A. P. Ramirez, T. Siegrist, G. Dabbagh, and S. E. Barrett, Nature **356**, 416 (1992).

[6] T. Yildirim, O. Zhou, J. E. Fischer, N. Bykovetz, R. A. Strongin, M. A. Cichy, A. B. Smith III, C. L. Lin, and R. Jelinek, Nature **360**, 568 (1992).

[7] R. C. Haddon, A. F. Hebard, M. J. Rosseinsky, D. W. Murphy, S. J. Duclos, K. B. Lyons, B. Miller, J. M. Rosamilia, R. M. Fleming, A. R. Kortan, S. H. Glarum, A. V. Makhija, A. J. Muller, R. H. Eick, S. M. Zahurak, R. Tycko, G. Dabbagh, and F. A. Theil, Nature **350**, 320 (1991).

[8] A. F. Hebard, M. J. Rosseinsky, R. C. Haddon, D. W. Murphy, S. H. Glarum, T. T. M. Palstra, A. P. Ramirez, and A. R. Kortan, Nature **350**, 600 (1991).

[9] M. J. Rosseinsky, A. P. Ramirez, S. H. Glarum, D. W. Murphy, R. C. Haddon, A. F. Hebard, T. T. M. Palstra, A. R. Kortan, S. M. Zahurak, and A. V. Makhija, Phys. Rev. Lett. **66**, 2830 (1991).

[10] K. Tanigaki, T. W. Ebbesen, S. Saito, J. Mizuki, J. S. Tsai, Y. Kubo, and S. Kuroshima, Nature **352**, 222 (1991).

[11] R. M. Fleming, A. P. Ramirez, M. J. Rosseinsky, D. W. Murphy, R. C. Haddon, S. M. Zahurak, and A. V. Makhija, Nature **352**, 787 (1991).

[12] P. W. Stephens, L. Mihaly, P. L. Lee, R. L. Whettenn, S. M. Huang, R. B. Kaner, F. Diederich, and K. Holczer, Nature **351**, 632 (1991).

[13] Q. Zhu, O. Zhou, N. Coustel, G. B. M. Vaughan, J. P. McCauley Jr., W. J. Romanow, J. E. Fischer, and A. B. Smith III, Science **254**, 545 (1991).

[14] R. M. Fleming, M. J. Rosseinsky, A. P. Ramirez, D. W. Murphy, J. C. Tully, R. C. Haddon, T. Siegrist, R. Tycko, S. H. Glarum, P. Marsh, G. Dabbagh, S. M. Zahurak, A. V. Makhija, and C. Hampton, Nature **352**, 701 (1991); see also Nature **353**, 868(E) (1991).

[15] O. Zhou, J. E. Fischer, N. Coustel, S. Kycia, Q. Zhu, A. R. McGhie, W. J. Romanow, J. P. McCauley Jr., A. B. Smith III, and D. E. Cox, Nature **351**, 462 (1991).

[16] Atsushi Oshiyama and Susumu Saito, Solid State Commun. **82**, 41 (1992).

[17] Jose Luis Martins and N. Troullier, Phys. Rev. B **46**, 1766 (1992).

[18] S. C. Erwin and W. E. Pickett, Science **254**, 842 (1991).

[19] Ming-Zhu Huang, Yong-Nian Xu, and W. Y. Ching, Phys. Rev. B **46**, 6572 (1992).

[20] M. P. Gelfand and J. P. Lu, Phys. Rev. Lett. **68**, 1050 (1992). A contrary result is given by R. P. Gupta and M. Gupta, Phys. Rev. B **47**, 11 635 (1993).

[21] R. Tycko, G. Dabbagh, R. M. Fleming, R. C. Haddon, A. V. Makhija, and S. M. Zahurak, Phys. Rev. Lett. **67**, 1886 (1991).

[22] R. Tycko, G. Dabbagh, M. J. Rosseinsky, D. W. Murphy, A. P. Ramirez, and R. M. Fleming, Phys. Rev. Lett. **68**, 1912 (1992).

[23] R. E. Walstedt, D. W. Murphy, and M. Rosseinsky, Nature **362**, 611 (1993).

[24] M. S. Deshpande and E. J. Mele (unpublished).

[25] E. J. Mele, in *Chemistry and Physics of Intercalation II* (Plenum, New York, in press).

[26] A recent nuclear magnetic resonance study concludes that if a model is isotropic, orientational dynamics is to be preferred to one of jumping between the two standard orientations. See S. E. Barrett and R. Tycko, Phys. Rev. Lett. **69**, 3754 (1992). However, it is not obvious to us that this interpretation is unique. In any event, as long as we can classify orientations as being nearly that of orientation A or nearly that of orientation B, our conclusions remain qualitatively valid.

[27] If one neglects quantum corrections, this argument indicates that M^+-$C_{60}{}^{3-}$ interactions can be neglected at zero temperature. At nonzero temperature, phonon modes (which do depend on such interactions) would give rise to effective C_{60}-C_{60} interactions, even if we completely neglected the direct C_{60}-C_{60} interactions. In the context of spin models, this phenomenon is referred to as "ordering due to disorder." See C. L. Henley, Phys. Rev. Lett. **62**, 2056 (1989), and references therein.

[28] Y. Guo, N. Karasawa, and W. A. Goddard III, Nature **351**, 464 (1991).

[29] M. Sprik, A. Cheng, and M. L. Kein, J. Phys. Chem. **96**,

2027 (1992).
[30] J. P. Lu, X.-P. Li, and R. M. Martin, Phys. Rev. Lett. **68**, 1551 (1992).
[31] R. Sachidanandam and A. B. Harris, Phys. Rev. Lett. **67**, 1467 (1991).
[32] P. A. Heiney, J. E. Fischer, A. R. McGhie, W. J. Romanow, A. M. Denenstien, J. P. McCauley, Jr., A. N. Smith III, and D. E. Cox, Phys. Rev. Lett. **67**, 1468 (1991).
[33] W. I. David, R. M. Ibberson, J. C. Matthewman, K. Prassides, T. J. Dennis, J. P. Hare, H. W. Kroto, R. Taylor, and D. R. M. Walton, Nature **353**, 147 (1991).
[34] S. Liu, Y.-J. Lu, M. M. Kappes, and J. A. Ibers, Science **254**, 408 (1991).
[35] K. H. Michel, J. R. D. Copley, and D. A. Neumann, Phys. Rev. Lett. **68**, 2929 (1992).
[36] X.-P. Li, J. P. Lu, and R. M. Martin, Phys. Rev. B **46**, 4301 (1992).
[37] T. Yildirim and A. B. Harris, Phys. Rev. B **46**, 7878 (1992).
[38] L. Pintschovius, B. Renker, F. Gompf, R. Heid, S. L. Chaplot, M. Haluska, and H. Kuzmany, Phys. Rev. Lett. **69**, 2662 (1992).
[39] S. Huant, J. R. Robert, G. Chouteau, P. Bernier, C. Fabre, and A. Rassat, Phys. Rev. Lett. **69**, 2666 (1992).
[40] T. Yildirim, A. B. Harris, S. C. Erwin, and M. R. Pederson, Phys. Rev. B **48**, 1888 (1993).
[41] In discussing the Coulomb interactions between charged C_{60} molecules, we neglect the distortion of the molecule due to the fact that it is embedded in an environment having only cubic symmetry. Under this assumption its lowest charge multipoles are its total charge, Q_0, and next its sixth order multipole, which in spherical harmonic notation is denoted Q_6^M (see Ref. 40). The interaction energy involving Q_0 is independent of which of the two standard orientations the molecules assume. Thus, the lowest order multipole interaction is that of order $(Q_6)^2$. Such an interaction between molecules is of order R^{-13}, where R is the distance between molecules.
[42] J. L. Lebowitz, M. K. Phani, and D. F. Styer, J. Stat. Phys. **38**, 413 (1985).
[43] C. L. Henley, J. Appl. Phys. **61**, 3962 (1987).
[44] T. Yildirim, A. B. Harris, and E. F. Shender (unpublished).
[45] D. E. Moncton, J. D. Axe, and F. J. DiSalvo, Phys. Rev. Lett. **34**, 734 (1975); W. D. McMillan, Phys. Rev. B **12**, 1189 (1979); A. B. Harris and A. J. Berlinsky, Can. J. Phys. **57**, 1852 (1979).
[46] It is important to know the sign of this rotation. The sign implied by Eqs. (A10)–(A12) was confirmed by private communication with the authors of Ref. 20, whom we thank for this information. Changing the sign of this rotation would change the signs of the x,x and y,y elements of the matrix in Eq. (A15). Comparison of Eqs. (A15) and (A13) show that with the proper choice of sign of rotation these A-A and A-B interactions differ in sign and thus we have an alloy in the strong disorder limit.